Spectrochimica Acta Part A: Molecular and Biomolecular Spectroscopy 152 (2016) 461–467

Contents lists available at ScienceDirect

Spectrochimica Acta Part A: Molecular and Biomolecular Spectroscopy

journal homepage: www.elsevier.com/locate/saa

Nanocap array of Au:Ag composite for surface-enhanced Raman scattering

Yongjun Zhang [a,*], Cong Wang [a], Jinpeng Wang [b], Lei Chen [a], Jia Li [a], Yang Liu [a], Xiaoyu Zhao [a], Yaxin Wang [a], Jinghai Yang [a,c]

[a] Key Laboratory of Functional Materials Physics and Chemistry, Jilin Normal University, Ministry of Education, Siping 136000, PR China
[b] Northeast Forestry University, Material Science and Engineering Institute, Harbin 150040, Heilongjiang, PR China
[c] Key Laboratory of Excited State Physics, Changchun Institute of Optics Fine Mechanics and Physics, Chinese Academy of Sciences, Changchun 130033, PR China

HIGHLIGHTS

- The co-sputtering Au:Ag bimetal array formed the protrusion network of Ag and Au nanoparticles.
- The metal protrusions in the waxberry-like shell contribute to the Raman enhancement.
- The SERS enhancements show the strong gap size-dependent behaviors.

GRAPHICAL ABSTRACT

In comparison to the curved Au/Ag bilayer, the Au:Ag bimetal arrays exhibit 4-fold more enhancement when Rhodamine 6G is chosen as the probing molecule.

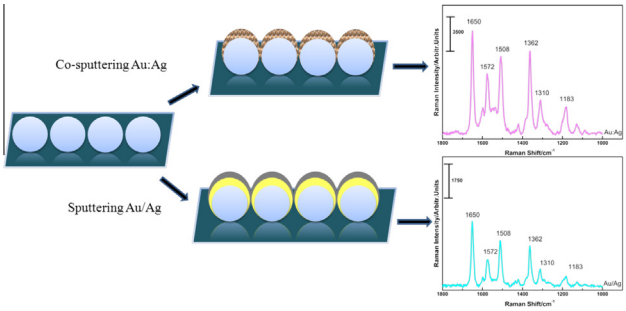

ARTICLE INFO

Article history:
Received 16 April 2015
Received in revised form 22 June 2015
Accepted 23 July 2015
Available online 29 July 2015

Keywords:
Surface-enhanced Raman scattering
Au:Ag nanocap
Nanogap
Local electric-field

ABSTRACT

We fabricated Au:Ag nanocap arrays by co-sputtering Au and Ag onto two-dimensional polystyrene (PS) colloidal sphere templates in a magnetron sputtering system for the surface-enhanced Raman scattering (SERS) substrate. In contrast to the bilayer Au/Ag, the co-sputtering Au:Ag bimetal array formed the protrusion network of Ag and Au nanoparticles, which contributed to Raman enhancement in the waxberry-like structure. The metal protrusions formed waxberry-like shell in which the PS beads were encapsulated. At the same time, the Au:Ag bimetal arrays exhibit 4-fold more enhancement in the SERS signal intensity of Rhodamine 6G at the 1649 cm^{-1} than Au/Ag bilayer array, which is ascribed to the plasmon coupling between the nanoparticles of Au and Ag on the sample. When the PS colloidal particle templates were etched by O_2-plasma before sputtering process, the nanogaps affected the surface plasmon resonance (SPR), and the optimal gaps between adjacent Au:Ag nanocaps generated even stronger SERS enhancements. This SERS substrate of Au:Ag showed high sensitivity and reproducibility. The EF of Au:Ag nanocap array substrate onto which Rhodamine 6G (R6G) were adsorbed was evaluated as 6.72×10^{10}.

1. Introduction

Surface-enhanced Raman scattering (SERS) is the one of the most effective detection methods for its high sensitivity, rapid

* Corresponding author.
E-mail address: jhyang1@jlnu.edu.cn (Y. Zhang).

http://dx.doi.org/10.1016/j.saa.2015.07.093
1386-1425/

response, noninvasive analysis, and fingerprint recognition [1–4]. There are two mechanisms to the enhancement of SERS, one is the chemical mechanism (CM) and the other is the electromagnetic mechanism (EM). The EM is considered as the main mechanism as the CM contributes merely 10–10^4 to single molecule enhancement while the EM gives 10^8 enhancement or even more. In the presence of plasmonic surface structures the EM fields can amplify the Raman scattering intensity due to surface plasmon resonance (SPR). SERS processes based on SPR have been widely used for the molecular recognition of chemicals and biomolecules [5]. A lot of articles have focused on optimizing the surface patterns of orderly arrayed metallic nanostructures. SPR can be tuned by adjusting the shape, size, environment, composition, and the nanogap in the metal nanostructure arrays [6–11]. Among these characteristics, the nanogap in the metal nanostructure arrays is one of the most significant factors for SERS responses because the coupling among adjacent metal nanostructures can amplify the local EM field enhancement [12–15]. Theoretical studies have shown that variations in particle–particle spacing affect the strength of these "gap plasmons" between nanoparticles. When the spacing sizes change as small as 1 nm, the SERS signal rise or fall by amounts as large as an order of magnitude [16,17].

However, the nonuniform distribution of "hot spots" and the randomly roughened metal surfaces that result in inhomogeneous distribution of target molecules provide challenges to obtaining SERS performance. Until today, a simple and reproducible method to fabricate metal nanostructures over a large area with high uniformity remains a major issue, and the studies on the reproducibility and uniformity of SERS substrates are concentrated on advanced nanopatterning techniques such as electron-beam lithography [18], electro-chemical metal growth [19], nanoimprint lithography [20], nanosphere lithography (NSL) [21–27], and so on. Compared to other methods, nanosphere lithography (NSL) is an economic, robust route and simple method for the fabrication of uniformly ordered nanostructure array over large area owing to its good wide size ranges, easy availability monodispersity [28–31]. In our previous reports, we fabricate the ordered nanogap arrays over large area by NSL and the approach could be extended to a wide range of coating materials, allowing controlled nanocap thickness and size, the size of the nanogap [32].

Since the discovery of SERS for the EM mechanisms about 30 years ago, the noble metal silver (Ag) and gold (Au) have been the promising materials as SERS-active substrate due to their remarkable surface plasmon characteristics. Ag is known to be the most effective metal for Raman signal enhancement due to its excitation being in the visible part of the electromagnetic spectrum. However, Ag is not regarded as a bio-compatible and stable material due to its strong oxidizing power [33]. In contrast, Au is a typical bio-compatible and chemical performance is stable material, but its SERS signal enhancement is relatively weaker than that of Ag.

In this paper, we fabricate a large-area, highly ordered Au:Ag nanocap array by co-sputtering Au and Ag onto two-dimensional PS colloidal particle templates in a magnetron sputtering system, and the Au:Ag nanocap arrays show good surface uniformity over large areas and size-dependence. When the PS colloidal particle templates are etched by O_2-plasma, the nanogap between nanocaps can be controlled by etching time. The large-area, highly ordered, and stable Au:Ag nanocap arrays lead to a large enhancement of SERS activity.

2. Experiment

2.1. Materials

Rhodamine 6G (R6G 96%) was obtained from Aladdin, 4-aminothiophenol (PATP), Sodium dodecyl sulfate and ethanol were purchased from Sigma–Aldrich Co., Ltd. at highest purity available and used as received without further purification. Au and Ag targets were purchased from Beijing TIANQI Advanced Materials Co., Ltd. (HZTQ). Silicon (Si) wafer and ultrapure water (18.0 Ω cm^{-1}) was used throughout the present study. The monodisperse polystyrene colloid particles were purchased from Duke (10 wt% aqueous solution).

2.2. Assemble of PS arrays

The two-dimensional (2D) ordered array of polystyrene colloids microsphere by self-assemble technique were fabricated on Si wafer. First, keep the thorough washed silicon substrates in 10%

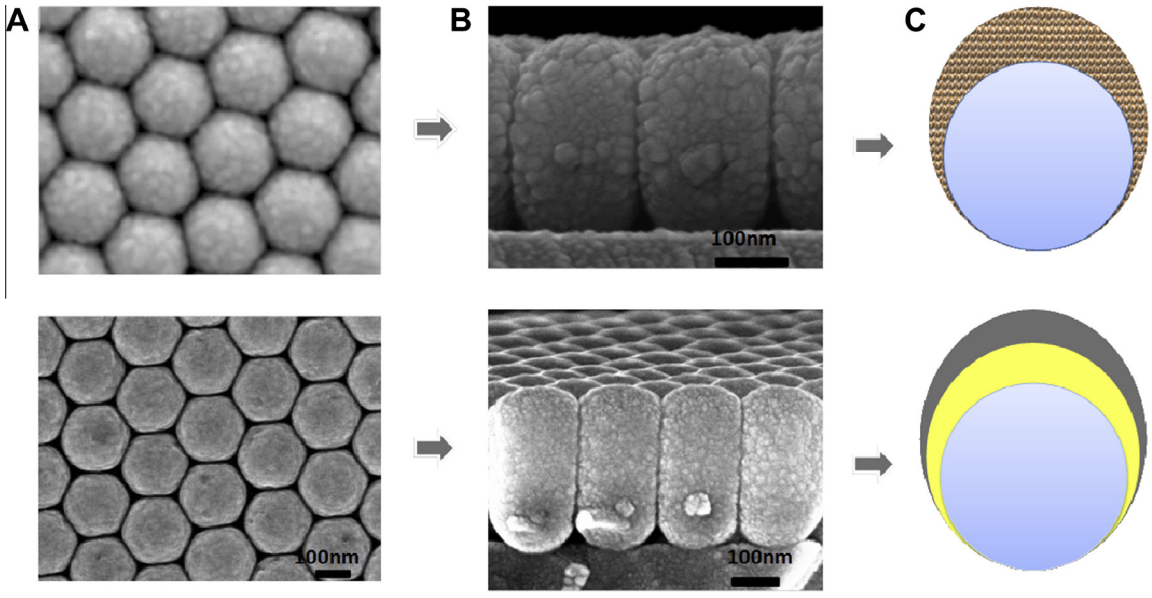

Fig. 1. The schematic diagram and SEM images. (A) The SEM images of Au:Ag nanocap array and Au/Ag bilayer on PS template. (B) The high enlarge SEM image of Au:Ag nanocap array and Au/Ag bilayer on PS template. (C) The schematic diagram of two structures.

sodium dodecyl sulfate solution for 24 h and the Si wafer becomes hydrophilic. Then, the Si wafer with diluted PS was slowly immersed into the glass vessel filled with water. The PS particles started to form an unordered monolayer on the water surface. After that, the sodium dodecyl sulfate solution was added onto the water surface, which drove the monolayer into highly ordered pattern. The monolayer of the close-packed 2D PS array was picked up by the hydrophilic Si wafer. The detailed process of the self-organization was reported in our previous work [34]. And the plasma cleaner (Model 1020, E.A. Fischione Instruments Inc.) was used to etch the two-dimensional (2D) array of PS microsphere, and the working gas was a mixture of 80% O_2 and 20% Ar.

2.3. Preparation of Au:Ag nanocap arrays

The Au:Ag nanocap arrays were fabricated on PS array by co-sputtering Au and Ag targets in magnetron sputtering system (ATC 1800-F, USA AJA). The distance between the substrate and target was 20 cm. During the deposition process the substrate was rotated, in a vacuum chamber with a base pressure of 1.8×10^{-6} Torr. The sputtering power of Ag and Ag targets were 20 w. During film deposition, the working air of argon pressure was 4.5×10^{-3} Torr.

2.4. Probe molecules absorption

We used the Rhodamine 6G (R6G) aqueous solution to evaluate the substrate Raman-enhancing capability. The sample was immersed in R6G the solution with concentration is 10^{-6} mol/L for 3 h and were washed thoroughly for three times with ethanol to remove unabsorbed R6G. The samples were finally gently dried with N_2 gas.

2.5. Characterization of substrates and SERS measurements

Raman spectra were measured using Renishaw inVia Raman system using a 514 nm Ar+ ion laser (20 mW) excitation. The Raman emissions, dispersed in a 0.5 m single monochromator equipped with a grating of 1800 grooves cm^{-1}, were detected with CCD. A 50 × 0.50 NA Leica object focused the excitation beam onto the samples using a spot size of ca 1 μm. The signal acquisition time was 10 s in a 180° backscattering geometry. According to manufacturer technical parameters, the solid angle of collection, Ω, was 0.37 steradians. The UV–Vis spectra of Au/Ag and Au:Ag were recorded on a UV-3600 spectrophotometer (Shimadzu). We used the scanning electron microscopy (SEM) to investigate the microstructure and morphology of the Au:Ag nanocap arrays. The SEM images were recorded on a JEOL 7800F, operating at 5.0 kV. And X-ray diffraction (XRD) patterns were recorded by a MAC Science MXP-18 X-ray diffractometer using a Cu target radiation source.

3. Result and discussion

The Au 20 nm/Ag 20 nm bilayer and Au:Ag 40 nm bimetal monolayer nanocaps are deposited on the closed-packed two-dimensional (2D) PS with 200 nm size arrays by alternatively sputtered and co-sputtered method respectively. The schematic diagram and SEM images in Fig. 1 show that the two samples both are in the perfect ordered hexagonal arrangements as PS beads array (Fig. 1A). In contrast to the bilayer, the co-sputtering Au:Ag bimetal array shows more roughness. Many metal protrusions form waxberry-like shell in which the PS beads are encapsulated so that the beads can hardly be seen, which indicates that the Au and Ag particles cover the surface of PS beads completely. The high enlarged SEM image in Fig. 1B shows that the particle size is about 10 nm to 20 nm, and the particle coalescence occurs so that some crevices exist in the sample, which is ascribed to the low substrate temperature during deposition process. The schematic diagram is given in Fig. 1C.

It is known that some nanoscale receives and sharp protrusions in metal nanostructures are the primary features to produce high Raman scattering enhancement of absorption molecules. To evaluate the contribution of the protrusion network of Ag and Au nanoparticles to Raman enhancement in the waxberry-like structure, the SERS spectra are measured and the results are shown in Fig. 2A. Compared to Au/Ag bilayer array, the Au:Ag bimetal arrays exhibit 4-fold enhancement in the SERS signal intensity of Rhodamine 6G at the 1649 cm^{-1}. In contrast to the Au/Ag bilayer array, the absorbance spectra of Au:Ag co-sputtering bimetal exhibits obvious differences (Fig. 2B). The spectrum of Au/Ag bilayer array contains two absorption bands around 350 nm and 580 nm corresponding to Ag and Au respectively, which indicates weak plasmon coupling between Au and Ag. However, the LSPR peaks for the co-sputtered Au:Ag bimetal array is broadened and

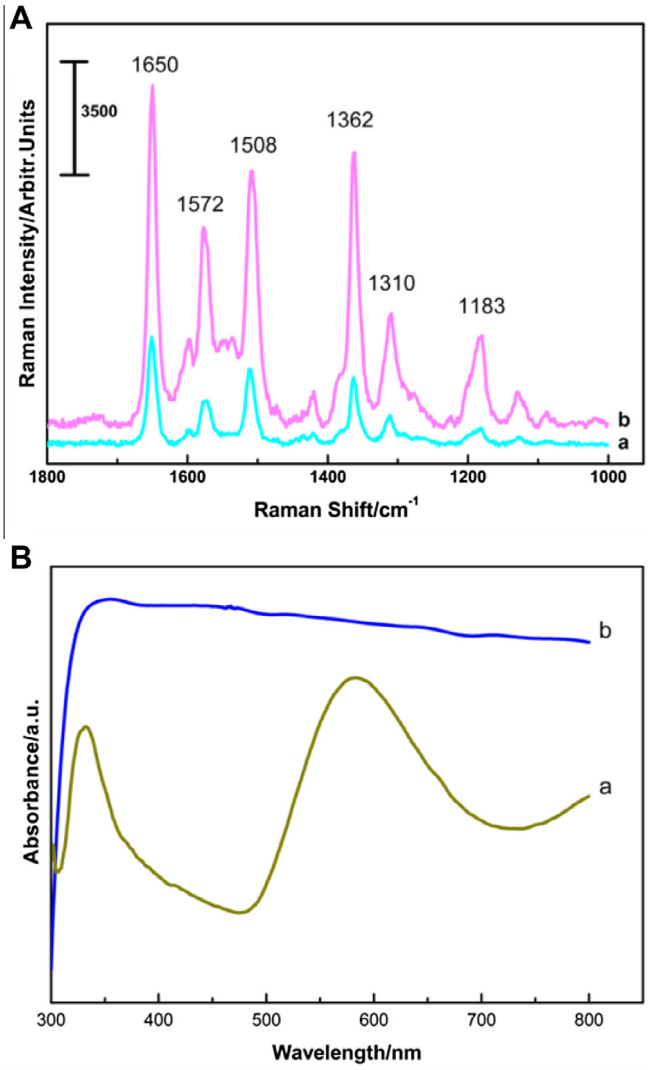

Fig. 2. (A) is the SERS spectra of 10^{-6} M R6G adsorbed on nanocaps, (a) 20 nm Au/20 nm Ag bilayer deposited on PS 200 nm templates, (b) 40 nm Au:Ag co-sputtering film deposited on PS 200 nm templates. (B) UV–Visible absorption spectrum for (a) 20 nm Au/20 nm Ag bilayer, (b) 40 nm Au–Ag co-sputtering film deposited on PS 200 nm template.

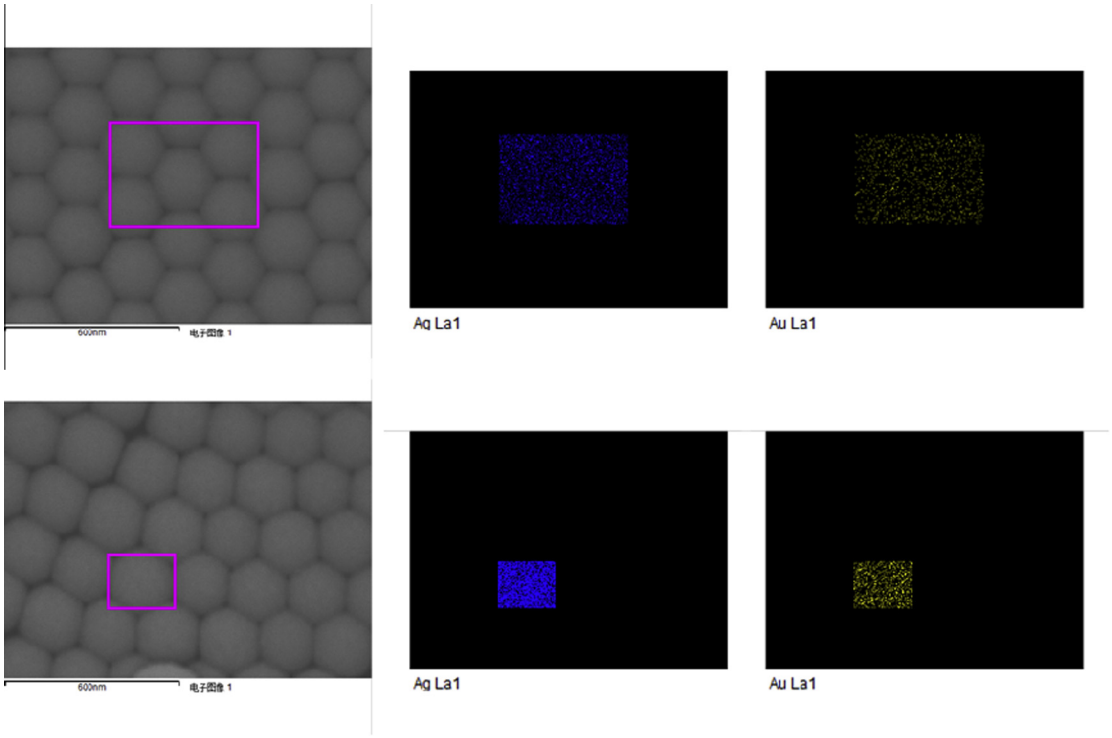

Fig. 3. The element analysis mapping of Au:Ag nanocap arrays by SEM. The blue and yellow colors are corresponding to silver and gold composition respectively. (For interpretation of the references to color in this figure legend, the reader is referred to the web version of this article.)

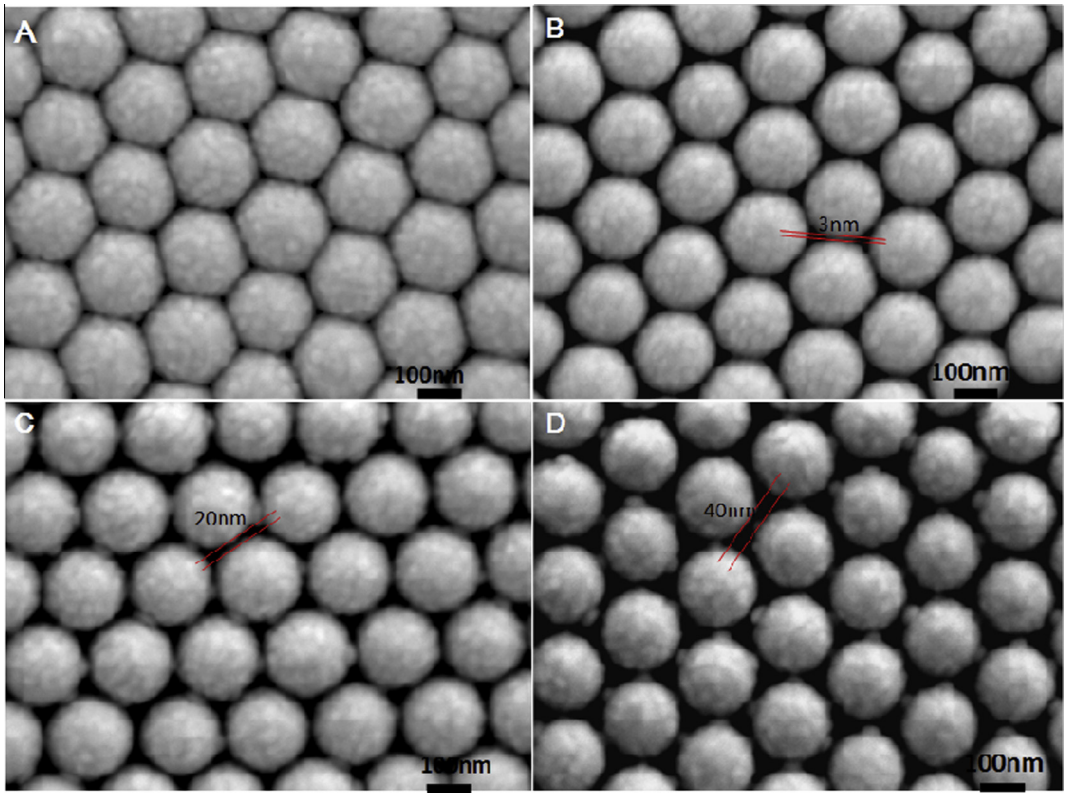

Fig. 4. SEM of the nanogaps arrays with the 40 nm Au:Ag film over polystyrene colloid sphere created by various etching time, and the anisotropic oxygen plasma etch time is (A) 0 s, (B) 30 s, (C) 60 s, (D) 120 s.

red/blue-shift across the visible spectrum and the NIR region, which is ascribed to the plasmon coupling between the nanoparticles of Au and Ag on the sample. The element analysis mapping on the surface of nanocap of Au:Ag bimetal arrays is

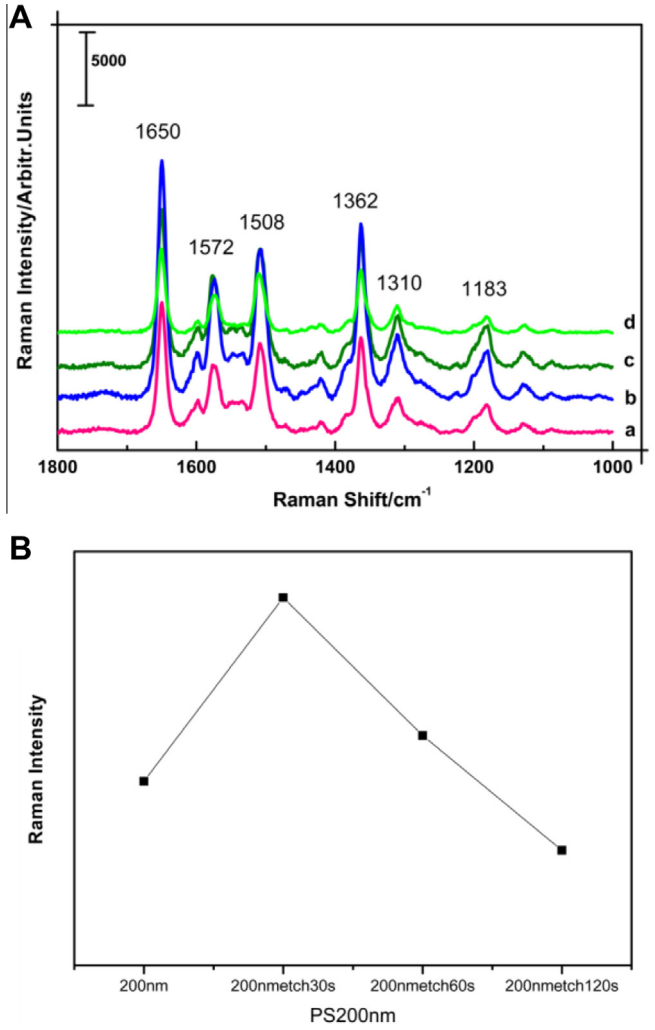

Fig. 5. (A) The SERS spectra of R6G adsorbed on 40 nm Au:Ag films over polystyrene colloid sphere with various etching time taken with 514 nm laser light (a) 0 s, (b) 30 s, (c) 60 s, (d) 120 s. (B) The corresponding dependence of the Raman signal intensity on etching time.

employed by SEM, and the result is shown in Fig. 3. The blue and yellow colors are corresponding to silver and gold composition respectively. It can be seen that the Au and Ag elements are distributed on the surface of the nanocap randomly. The existence of Au composition can provide more possibilities to trap detecting molecules due to the excellent compatibility and these molecules can excite particularly large enhancements of the electromagnetic field by Ag composition. Therefore, we believe that the network of Au and Ag on waxberry-like structured surface contribute to the large SERS enhancement in co-sputtered bimetal Au:Ag array.

Except for the crevices consist of Ag and Au nanoparticles, the nanogap between adjacent PS beads also contribute to SERS enhancement [21]. To investigate the contribution of nanogap between adjacent nanocaps to SERS, the nanogaps are created by adjusting 2D PS arrays. Fig. 4 shows SEM images of co-sputtering bimetal Au:Ag array with different nanogaps. On the original template of 200 nm PS array without gaps, Au:Ag nanocap array shows closely packed structure. When the PS beads templates are etched by O_2-plasma, the nanogaps appear between adjacent nanocaps. With the increase of etching time from 30 s to 120 s, the sizes of nanogaps vary from approximately 3 nm to 40 nm. Fig. 5 shows the SERS spectra change with etching times for the Au:Ag array. The intensity of the Raman signals obtained clearly depends on the etching time. When the etching time is 30 s, the nanogap is about 3 nm, the Raman peak shows the significant increase. Compared to the array without etching process, the SERS intensity is enhanced over 2 times. The additional enhancement is attributed to the large local electric fields generated in the nanogap adjacent nanocaps, which enhances the Raman excitation of the detecting molecule. When etching time increases over 60 s, the size of nanogap is larger than 20 nm, the Raman peak intensity gradually becomes weak, which is caused by the fact that the plasmon coupling between the adjacent nanocaps is weakened at larger separation distances [35,36]. These results indicate that in our system the maximum optimized SERS performance can be obtained in bimetal Au:Ag nanocap array with the 3 nm gaps size, and Au and Ag nanoparticles on the surface of PS along with the gaps between adjacent PS beads play the same role in SERS enhancement.

The XRD images of samples are shown in Fig. 6. All the observed diffraction peaks can be indexed to Au and Ag with face-centered cubic structure according to JCPDS card No. 04-0784 and No. 04-0783, respectively. The diffraction peaks at 38.1°, 44.2°, 64.4°,

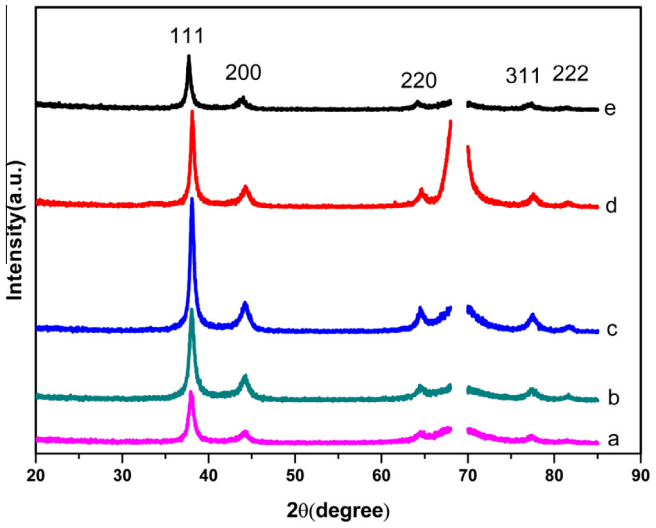

Fig. 6. XRD patterns of samples (a) 40 nm Au:Ag co-sputtering film deposited on PS 200 nm templates. (b) 20 nm Au/20 nm Ag bilayer deposited on PS 200 nm templates. (c)–(e) 40 nm Au:Ag film over polystyrene colloid sphere created by various etching time, and the anisotropic oxygen plasma etch time is 30 s, 60 s, 120 s.

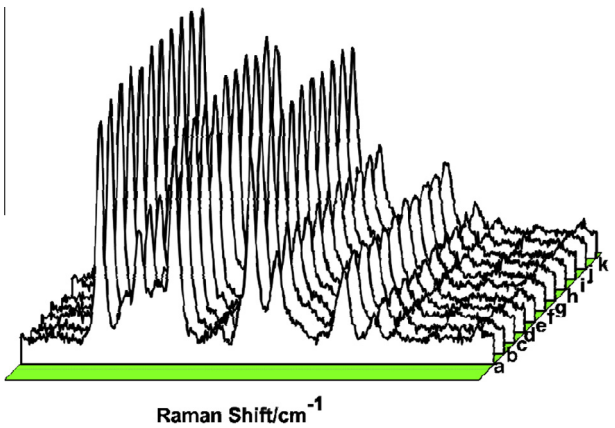

Fig. 7. The SERS spectra of R6G adsorbed on 40 nm Au:Ag films at 11 random positions across a 4 cm^2 substrate.

77.4° and 81.5° 2θ, correspond to the (111), (200), (220), (311), and (222) lattices in Au and Ag, which indicate no other impurity phase exists in the samples. The lattice parameters of Au and Ag are basically the same, therefore the diffraction peaks are overlapped completely. For the five samples, the strong peak at 69.14° is from the Si substrate.

3.1. SERS enhancement factor (EF) of bimetal Au:Ag nanocap arrays

The enhancement factors (EFs) for PATP and R6G is calculated according to the equation $EF = (I_{SERS} \times N_{bulk})/(I_{bulk} \times N_{ads})$, where I_{SERS} and I_{bulk} are the SERS intensity of the bands at 1072 cm^{-1} for PATP absorbed on Au:Ag arrays and the Raman intensity of the band at 1090 cm^{-1} for the solid PATP, respectively (Supporting information) [37,38]. The average number of molecules in the scattering volume (V) for the Raman (non-SERS) measurement is $N_{bulk} = C_{RS}VN_A$. The molar concentration (C_{RS}) of the PATP analyte on the reference region is 1 mM. N_{ads} is the average number of adsorbed molecules in the scattering volume for the SERS experiments. $N_{ads} = N_d\ A_{laser}\ AN/\sigma$ where N_d is the number density of PS with diameter 200 nm, A_{laser} is the area of the focal laser spot. The laser spot is a circle with a diameter of 1 μm. AN is the half surface area of one PS with diameter 200 nm, and σ is the surface area occupied by a single PATP adsorbed on the substrate value, which is estimated to be 0.20 nm^2 [39]. For the Renishaw Micro-Raman spectrometer with the 514.5 nm laser excitation, the effective focused depth is 19 μm. N_{bulk} and N_{ads} can be calculated to be 8.46×10^{10} and 7.85×10^6, respectively. $I_{SERS} = 10923.8978$, $I_{bulk} = 1752.3168$. EF is calculated to be 6.72×10^4 for 40 nm Au and Ag co-sputtered nanocap substrate at the band of 1072 cm^{-1} of the PATP analyte. In this work, the ratio of the Raman intensities of the R6G and thiol related C–C stretching bands at R6G saturation coverage is about 1×10^6, as reported by Tao et al. [40]. Using this ratio and the EF for PATP, the EF for R6G is estimated to be 6.72×10^{10} for Au and Ag co-sputtered nanocap substrate [41].

We study the reproducibility of SERS substrate for the bimetal Au:Ag nanocap on PS 200 by measuring random spots across the whole nanocap array. Fig. 7 shows the SERS spectra collected from 11 random positions across a 4 cm^2 substrate. The maximum standard deviation of the intensity is calculated to be 10.7% with respect to the average intensity of the band at 1649 cm^{-1}, indicating the SERS enhancements are uniform across the sample surface. The homogenous and high-ordered bimetal Au:Ag nanocap arrays can provide a promising application in biosensor and quantitative analysis of spectroscopy.

4. Conclusions

In this work, we report the fabrication of Au:Ag nanocap arrays substrate with fine surface uniformity and a tunable adjacent gap by Au and Ag co-deposition onto 2D polystyrene colloid sphere template. The co-sputtering Au:Ag bimetal array formed the protrusion network of Ag and Au nanoparticles. In the Au:Ag composite arrays, the metal protrusions form waxberry-like shell and the PS beads are encapsulated. In contrast to the bilayer, the Au:Ag bimetal arrays exhibit 4-fold more enhancement in the SERS signal intensity of Rhodamine 6G than Au/Ag bilayer array due to the plasmon coupling between the nanoparticles of Au and Ag. And the SERS enhancements also show the strong gap size-dependent behaviors. The highly ordered Au:Ag nanocap arrays provide high sensitivity, bio-compatible and stable of SERS based detections, resulting in a high performance of the SERS substrate.

Acknowledgements

This work is supported by Program for New Century Excellent Talents in University (Nos. NCET-09-0156 and NCET-11-0981) and Program for the development of Science and Technology of Jilin province (Nos. 20120359 and 20140519003JH), Program for the master students' scientific and innovative research of Jilin Normal University (No. 201109).

Appendix A. Supplementary data

Supplementary data associated with this article can be found, in the online version, at http://dx.doi.org/10.1016/j.saa.2015.07.093.

References

[1] L. Guerrini, D. Graham, Chem. Soc. Rev. 41 (2012) 7085–7107.
[2] D. Tsoutsi, J.M. Montenegro, F. Dommershausen, U. Koert, L.M. Liz-Marzán, W.J. Parak, R.A. Alvarez-Puebla, ACS Nano 5 (2011) 7539–7546.
[3] C.L. Zavaleta, B.R. Smith, I. Walton, W. Doering, G. Davis, B. Shojaei, M.J. Natan, S.S. Gambhir, Proc. Natl. Acad. Sci. U.S.A. 106 (2009) 13511–13516.
[4] Y.C. Cao, R. Jin, C.A. Mirkin, Science 297 (2002) 1536–1540.
[5] J.F. Li, Y.F. Huang, Y. Ding, Z.L. Yang, S.B. Li, X.S. Zhou, F.R. Fan, W. Zhang, Z.Y. Zhou, D.Y. Wu, B. Ren, Z.L. Wang, Z.Q. Tian, Nature 464 (2010) 392–395.
[6] W.A. Murray, W.L. Barnes, Adv. Mater. 19 (2007) 3771–3782.
[7] C. D'Andrea, J. Bochterle, A. Toma, C. Huck, F. Neubrech, E. Messina, B. Fazio, O.M. Marago, E.D. Fabrizio, P.G. Gucciardi, A. Pucci, ACS Nano 7 (2013) 3522–3531.
[8] J.J. Mock, M. Barbic, D.R. Smith, D.A. Schultz, S. Schultz, J. Chem. Phys. 116 (2002) 6755–6759.
[9] C.J. Heo, S.H. Kim, S.G. Jang, S.Y. Lee, S.M. Yang, Adv. Mater. 21 (2009) 1726–1731.
[10] J. Ye, F. Wen, H. Sobhani, J.B. Lassiter, P.V. Dorpe, P. Nordlander, N.J. Halas, Nano Lett. 12 (2012) 1660–1667.
[11] A.D. Falco, M. Ploschner, T.F. Krauss, New J. Phys. 12 (2010) 113006.
[12] S.S. Acimovic, M.P. Kreuzer, M.U. Gonzalez, R. Quidant, ACS Nano 3 (2009) 1231–1237.
[13] B. Yan, A. Thubagere, W.R. Premasiri, L.D. Ziegler, L.D. Negro, B.M. Reinhard, ACS Nano 3 (2009) 1190–1202.
[14] A. Tao, P. Sinsermsuksakul, P. Yang, Nat. Nanotechnol. 2 (2007) 435–440.
[15] C.J. Heo, H.C. Jeon, S.Y. Lee, S.G. Jang, S. Cho, Y. Choi, S.M. Yang, J. Mater. Chem. 22 (2012) 13903.
[16] M. Futamata, Y. Maruyama, M. Ishikawa, J. Phys. Chem. B 107 (2003) 7607–7617.
[17] K.D. Alexander, M.J. Hampton, S.P. Zhang, A. Dhawan, H.X. Xu, R. Lopez, J. Raman Spectrosc. 40 (2009) 2171–2175.
[18] L. Gunnarsson, E.J. Bjerneld, H. Xu, S. Petronis, B. Kasemo, M. Kall, Appl. Phys. Lett. 78 (2001) 802–804.
[19] A. Gopinath, S.V. Boriskina, W.R. Premasiri, L. Ziegler, B.M. Reinhard, L.D. Negro, Nano Lett. 9 (2009) 3922–3929.
[20] S.Y. Chou, P.R. Krauss, P.J. Renstrom, Science 272 (1996) 85–87.
[21] H. Wang, C.S. Levin, N.J. Halas, J. Am. Chem. Soc. 127 (2005) 14992–14993.
[22] C.L. Haynes, R.P. Van Duyne, J. Phys. Chem. B 105 (2001) 5599–5611.
[23] S.H. Lee, K.C. Bantz, N.C. Lindquist, S. Oh, C.L. Haynes, Langmuir 25 (2009) 13685–13693.
[24] L.A. Dick, A.D. McFarland, C.L. Haynes, R.P. Van Duyne, J. Phys. Chem. B 106 (2002) 853–860.
[25] Y. Lu, G.L. Liu, J. Kim, Y.X. Mejia, L.P. Lee, Nano Lett. 5 (2005) 119–124.
[26] R.P. Van Duyne, J.C. Hulteen, D.A. Treichel, J. Chem. Phys. 99 (1993) 2101–2115.
[27] C.X. Wang, W.D. Ruan, N. Ji, W. Ji, S. Lv, C. Zhao, B. Zhao, J. Phys. Chem. C 114 (2010) 2886–2890.
[28] X.L. Li, Y.Z. Zhang, Z.X. Shen, H.J. Fan, Small 8 (2012) 2548–2554.
[29] S. Guddala, S.A. Kamanoor, A. Chiappini, M. Ferrari, N.R. Desai, J. Appl. Phys. 112 (2012) 084303.
[30] A.D. McFarland, M.A. Young, J.A. Dieringer, R.V. Duyne, J. Phys. Chem. B 109 (2005) 11279–11285.
[31] D.A. Stuart, J.M. Yuen, N. Shah, O. Lyandres, C.R. Yonzon, M.R. Glucksberg, J.T. Walsh, R.V. Duyn, Anal. Chem. 78 (2006) 7211–7215.
[32] Y.J. Zhang, L.X. Sun, Y.X. Wang, X. Ding, Y. Cheng, J.H. Yang, Solid State Commun. 147 (2008) 262.
[33] H.W. Yoo, J.M. Jung, S.K. Lee, H.T. Jung, Nanotechnology 22 (2011) 095304.
[34] Y.J. Zhang, W. Li, J. Li, Y.M. Zhang, Y.X. Wang, S.Y. Yang, S.S. Liu, J. Appl. Phys. 111 (2012). 053925-053925-6.
[35] B.Y. Lee, K. Heo, A.L. Schmucker, H.J. Jin, J.K. Lim, T. Kim, H. Lee, K.S. Jeon, Y.D. Suh, C.A. Mirkin, S. Hong, Nano Lett. 12 (2012) 1879–1884.
[36] H. Kang, C.J. Heo, H.C. Jeon, S.Y. Lee, S.M. Yang, Nano Lett. 10 (2010) 4488–4493.
[37] Z. Zhu, C. Fan, J. Wang, J. He, E. Liang, M. Chao, J. Appl. Phys. 116 (2014) 044312.

[38] B. Ren, X.F. Lin, Z.L. Yang, G.K. Liu, R.F. Aroca, B.W. Mao, Z.Q. Tian, J. Am. Chem. Soc. 125 (2003) 9598–9599.
[39] J. Jiang, K. Bosnick, M. Maillard, L. Brus, J. Phys. Chem. B 107 (2003) 9964–9972.
[40] A. Tao, F. Kim, C. Hess, J. Goldberger, R. He, Y.G. Sun, Y.N. Xia, P.D. Yang, Nano Lett. 3 (9) (2003) 1229–1233.
[41] G. Wei, L. Wang, Z.G. Liu, Y.H. Song, L.L. Sun, T. Yang, Z. Li, J. Phys. Chem. B 109 (50) (2005) 23941–23947.